HARDWARE TECHNIQUES FOR IMPROVING THE CALIBRATION PERFORMANCE OF DIRECT RESISTIVE SENSOR-TO-MICROCONTROLLER INTERFACE

Zivko Kokolanski, Cvetan Gavrovski, Vladimir Dimcev, **Mario Makraduli**

Ss. Cyril and Methodius University, Faculty of Electrical Engineering and Information Technologies, Ruger Boskovic bb, 1000 Skopje, Republic of Macedonia (✉ kokolanski@feit.ukim.edu.mk)

Abstract

Direct sensor-to-microcontroller is a simple approach for direct interface of passive modulating sensors to a microcontroller without any active components in between the sensor and the microcontroller and without an analog to digital converter. The metrological performances of such interface circuits are limited by certain microcontroller parameters which are predetermined by the manufacturing technology. These limitations can be improved by specific hardware-related techniques and can improve the accuracy, speed and resolution of the measurements. Such hardware solutions as well as proper selection of the electrical components are addressed in this paper. It has been shown that employment of only a few MOSFET transistors can reduce the maximal relative error of single point calibration more than fifteen times and can increase the measuring speed around 30 % in all calibration techniques in the measurement range of PT1000 resistive temperature sensors. Moreover, the effective number of resolution bits increases by more than 1.3 bits when using an external comparator.

Keywords: passive sensors, sensor interface, calibration, microcontroller.

1. Introduction

The rapid development of digital systems for measurement, processing and control makes digital sensors very attractive. These kinds of sensors have a digital output which simplifies the interface with digital systems. Moreover, they are less sensitive to electromagnetic interference comparing to the analog sensors.

In recent years a number of papers have been published on direct interface of passive sensors (resistive and capacitive) to digital programmable devices, such as microcontrollers [1], CPLD's and FPGA's [2]. These interfaces provide passive sensors to act like quasi-digital sensors and allow them to interface with digital systems directly i.e. without an analog to digital (AD) converter. These features make this kind of sensor interfaces attractive for low cost and miniature measurement system solutions [3, 4].

The most basic direct sensor-to-microcontroller interface can be realized by using two microcontroller ports, one input and one output port. The measurement contains two phases: a charging phase (Fig. 1a), and a discharging phase (Fig. 1b). In the charging phase, the port P_i is set as output in a "high" logic state and the port P_o is in high impedance state. The capacitor charges through the protection resistor (R_p) to the "high" voltage level (V_{oh}) in a period t_1 to t_2 shown in Fig. 1c. In the discharging phase (t_2 to t_3 in Fig. 1c), port P_o is set as the output in a "low" logic state, port P_i is configured as the input, and the microcontroller timer is active. This time the capacitor discharges through the sensor (R_x) until its voltage reaches the lower threshold voltage (V_{tl}) of P_i, when the timer is stopped. The time needed for the capacitor to discharge from V_{oh} to V_{tl} is:
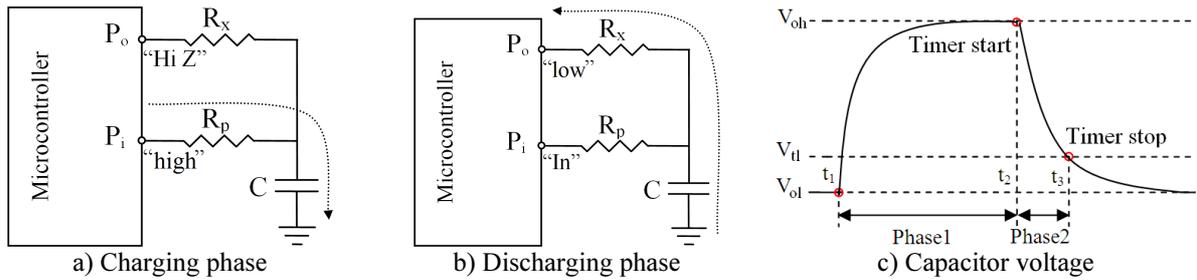
a) Charging phase   b) Discharging phase   c) Capacitor voltage

Fig. 1. Direct sensor-to-microcontroller interface.

$$t_x = R_x C \ln\left(\frac{V_{oh} - V_{ol}}{V_{tl} - V_{ol}}\right) = kR_x, \tag{1}$$

where, V_{ol} is the "low" voltage level of the digital output port. Considering V_{ol}, V_{oh}, V_{tl} and C as constants, from (1) it can be seen that the time interval t_x is proportional to the sensor resistance R_x. However, usually the constant k in (1) is not very stable due to temperature dependence and aging effects. Moreover, the input/output resistances and leakage currents of the microcontroller ports cause gain, offset and nonlinearity errors [5]. These effects can be reduced by using some calibration technique that yields a measurement result which depends on one or two calibration components rather than on the parameters mentioned above. In the literature, three calibration techniques are proposed: single point calibration [5]; two point calibration [5]; and the three signals method [6, 1]. Each of these calibration techniques has its own advantages in terms of simplicity, accuracy, cost and speed. Hence, in particular cases, a different calibration technique is more suitable and takes precedence over the others. However, generally the calibration performances are limited by the parameters of the digital programmable device ports and by specific calibration implementation-related issues. These limiting factors can be reduced by using external electrical components and can improve the overall performance of all mentioned calibration techniques. Such solutions, their metrological performances as well as proper selection of the external components are addressed in this paper.

2. Calibration

The simplified representation of single point calibration, two point calibration and the three signals method applied on direct sensor-to-microcontroller interface is given in Fig. 2a, Fig. 2b and Fig. 2c respectively.
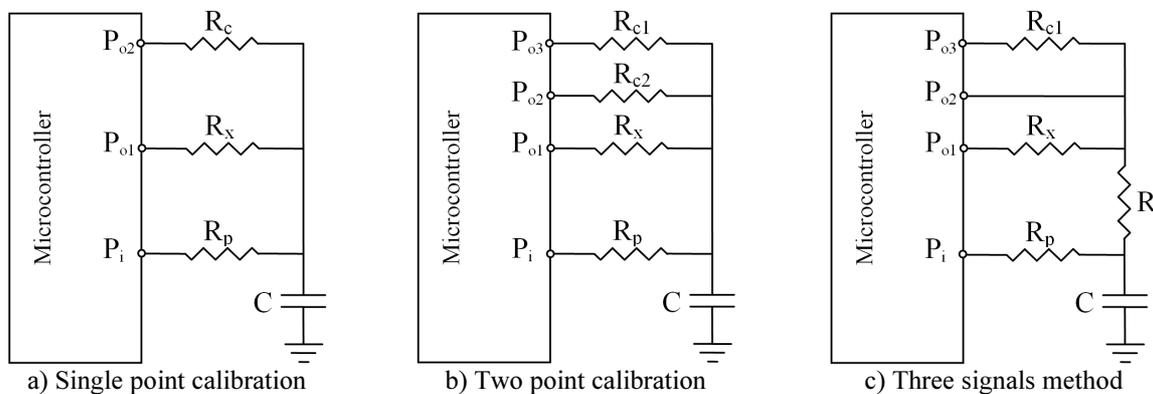

a) Single point calibration   b) Two point calibration   c) Three signals method

Fig. 2. Calibration techniques in direct sensor-to-microcontroller interface.

www.czasopisma.pan.pl PAN www.journals.pan.pl

POLSKA AKADEMIA NAUK

Metrol. Meas. Syst., Vol. XX (2013), No. 4, pp. 529–542.

2.1. Single point calibration

The single point calibration (SPC) given in Fig. 2a is the simplest one of all calibration techniques containing only one additional calibration resistor R_c. The measurement is performed in two phases: measurement of the sensor resistance R_x and measurement of the calibration resistance R_c. Each phase contains two sub-phases: charging sub-phase through R_p and discharging sub-phase trough R_x or R_c. Since the charging sub-phase carries no information about the measuring quantity, it should be short enough to increase the speed of the measurement. Typical duration of the charging sub-interval is five to seven times the charging time constant. In the discharging sub-phases, the capacitor voltage varies between V_{oh} and V_{tl}, and the output pulse width depends on the time needed to discharge the capacitor C through R_x or R_c. Since V_{oh}, V_{ol}, V_{tl} and C are the same in both discharging sub-phases, calculating the ratio of the discharging time intervals cancels their contribution, which is k in (1). The result is:

$$\frac{t_x}{t_c} = \frac{R_x C \ln\left(\frac{V_{oh} - V_{ol}}{V_{tl} - V_{ol}}\right)}{R_c C \ln\left(\frac{V_{oh} - V_{ol}}{V_{tl} - V_{ol}}\right)} = \frac{R_x}{R_c}, \tag{2}$$

where, t_x and t_c are the discharging time intervals through R_x and R_c respectively. From (2) the estimated sensor resistance is:

$$R_{x1p} = \frac{t_x}{t_c} R_c. \tag{3}$$

Equation (3) shows that the single point calibration treats the sensor resistance as a linear function by the product of the time intervals t_x and t_c and the calibration resistor R_c.

2.2. Two point calibration

The two point calibration given in Fig. 2b uses two calibration resistors: R_{c1} and R_{c2}. Therefore, the measurement is performed in three phases: measurement of the sensor resistance R_x and measurement of the calibration resistances R_{c1} and R_{c2}. This time, R_x is estimated as a two point line fit as follows:

$$\frac{t_x - t_{c2}}{t_{c1} - t_{c2}} = \frac{(R_x - R_{c2}) C \ln\left(\frac{V_{oh} - V_{ol}}{V_{tl} - V_{ol}}\right)}{(R_{c1} - R_{c2}) C \ln\left(\frac{V_{oh} - V_{ol}}{V_{tl} - V_{ol}}\right)} = \frac{(R_x - R_{c2})}{(R_{c1} - R_{c2})}. \tag{4}$$

Expressing the sensor resistance from (4) results in:

$$R_{x2p} = \frac{t_x - t_{c2}}{t_{c1} - t_{c2}}(R_{c1} - R_{c2}) + R_{c2}. \tag{5}$$

As with the single point calibration, the measured sensor resistance (5) is not affected by variation of the capacitance value C as well as by variations of the voltages V_{ol}, V_{oh} and V_{tl}. However, this time we have to know the values of two calibration resistors, R_{c1} and R_{c2} in (5) rather than one, R_c in (3).

2.3. Three signals method

The three signals method given in Fig. 2c is a special case of two point calibration where $R_{c2}=0$. Hence, the equation (5) becomes:

$$R_{x3sm} = \frac{t_x - t_{c2}}{t_{c1} - t_{c2}} R_{c1}.$$ (6)

The resistor R in Fig. 2c is used to limit the discharge current of the microcontroller port P_{o2}.

3. Improving the calibration performance with external electrical components

3.1. Accuracy

All calibration techniques described in the previous chapter are introducing systematic errors in the form of: gain, offset and nonlinearity [5]. These errors come mainly from the input/output resistances and leakage currents of the microcontroller ports. Moreover, the offset and gain components come mainly from the output resistances of the microcontroller ports and the nonlinearity errors from the input resistances and the leakage currents. However, the difference of (3), (5) and (6) leads to different performance of each calibration technique regarding the sources of errors mentioned above.

To evaluate the offset and the gain components of each calibration technique we define the output ports resistances as: R_{o1} for the port P_{o1}; R_{o2} for P_{o2}; and R_{o3} for P_{o3}. These resistances enlarge the discharging intervals t_x, t_{c1} and t_{c2} in (3), (5) and (6) because they appear in series with the resistors R_x, R_{c1} and R_{c2}. Thus, the equation (3) for single point calibration becomes:

$$R_{x1p} = \frac{R_c}{R_c + R_{o2}} R_x + \frac{R_c R_{o1}}{R_c + R_{o2}} = c_1' R_x + c_2'.$$ (7)

From (7), $R_{x1p}=R_x$ only when $R_x=R_c$, and if the output ports P_{o1} and P_{o2} are ideally matched i.e. $R_{o1}=R_{o2}$. As the difference between the sensor resistance R_x and the calibration resistance R_c increases, the systematic errors in the form of gain (c_1') and offset (c_2') increase. Similarly, for the two point calibration, when taking into account the output resistances of the microcontroller ports, the estimated sensor resistance (5) becomes:

$$R_{x2p} = \frac{R_{c1} - R_{c2}}{R_{c1} - R_{c2} + R_{o3} - R_{o2}} R_x + \frac{R_{c2}(R_{o3} - R_{o1}) - R_{c1}(R_{o2} - R_{o1})}{R_{c1} - R_{c2} + R_{o3} - R_{o2}} = c_1'' R_x + c_2''.$$ (8)

Equation (8) is directly applicable to the three signals method when considering $R_{c2}=0$. In the two point calibration and the three signals method, the gain (c_1'') and the offset (c_2'') components in (8) are on the order of the mismatch between the output port resistances. Therefore, if we have ideally matched ports i.e. $R_{o1}=R_{o2}=R_{o3}$, the gain and offset will be zero regardless of the sensor resistance value. Moreover, even if the microcontroller ports are not

ideally matched, the offset and gain components will be significantly lower than those of the single point calibration. To compensate for the wire resistance, the wire length connecting the sensor, the calibration resistors and the wire between P_{o2} and R in Fig. 2.c should be equal.

To reduce the offset and gain errors in single point calibration we propose a modification of the circuit given in Fig. 2.a with that given in Fig. 3. Thus, the sensor and the calibration resistor are driven by two external MOSFET transistors T_1 and T_2 instead of a direct connection to the microcontroller ports. In such case (7) becomes:

$$R_{x1p} = \frac{R_c}{R_c + R_{dson2}} R_x + \frac{R_c R_{dson1}}{R_c + R_{dson2}},$$ (9)

where R_{dson1} and R_{dson2} are the drain-to-source ON resistance of T_1 and T_2 respectively.
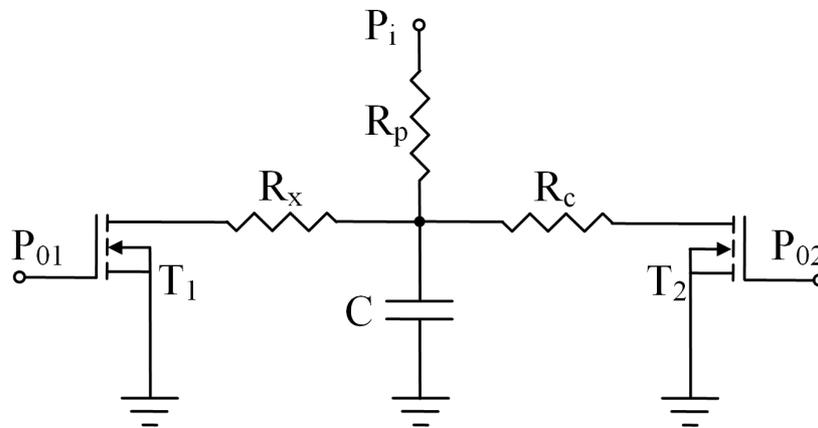

Fig. 3. Improving the accuracy of single point calibration with external electrical components.

The improvement contributed by the two MOSFET's is that in this case the parameters of the transistors determine the performance of single point calibration instead of the microcontroller ports whose parameters are predetermined by the manufacturing technology. Hence, if we select low drain-to-source ON resistance transistors for T_1 and T_2, the following approximation can be made:

$$R_{dson1} \approx R_{dson2} \approx 0 \Big|_{V_{oh} > V_{TH}},$$ (10)

where V_{TH} is the gate-to-source threshold voltage. This approximation yields $R_{x1p} = R_x$ in (7), thus completely removing the offset and gain systematic errors. Current technology enables manufacturing MOSFET transistors with R_{dson} in the order of several tenths of milliohms which makes approximation (10) quite reasonable. As a comparison, the output resistances of the microcontroller ports are usually in the order of tenths of ohms, which is roughly hundreds times higher than the R_{dson} of currently available MOSFET transistors. On the other hand, the offset and gain components greatly affect low resistance measurements and they decrease for higher resistance values where nonlinearity errors are dominant. In [5], the authors suggest that the nonlinearity errors are caused mainly by the input resistances and leakage currents of the microcontroller ports. Therefore, for higher resistor values or for sensors varying over a wide measurement range a better solution would be to use JFETs

for T_1 and T_2 in Fig. 3 with a little modification of the driving stage. The leakage currents of the JFETs are in the order of pA to nA, whereas in MOSFETs they are in the order of μA and yet increasing with temperature. Such solutions with JFETs could also reduce nonlinearity errors of the two point calibration and the three signals method. An alternate conclusion would be that substituting T_1 and T_2 in Fig. 3 with reed-relays would completely remove the offset, gain and nonlinearity errors since the on-state resistance and off-state leakage currents are zero. However, the long and unpredictable propagation delay along with a mechanically-dependent parameter and limited mechanical lifecycle makes reed-relays inappropriate for such applications.

Besides improvement in accuracy, the modified circuit given in Fig. 3 provides additional benefits when measuring low-resistance sensors. Namely, the minimal sensor resistance that can be directly measured with the basic interface circuit as given in Fig. 1 is:

$$R_{x\min} \geq \frac{V_{oh}}{I_{s\max}}, \tag{11}$$

where V_{oh} is the logic "high" voltage level and I_{smax} is the maximal current sunk by the microcontroller port. Having in mind that I_{smax} is typically around 25mA, the minimal sensor resistance would be around 200 ohms for a 5V microcontroller, which is quite restrictive. In such case, a low resistance strain gauge could be measured only with an additional shunt resistor which would decrease the measuring speed. On the other hand, MOSFET transistors with pulsed source currents of several amperes are nowadays easily available providing the possibility to directly measure sensor resistances as low as several ohms.

3.2. Measuring speed

The measuring speed is a very important parameter since it defines the system's overall bandwidth. Even when the measuring speed is not critical, the ability to perform faster measurements could be used to perform averaging and to reduce noise effects. In cases when the measurements are affected by Gaussian noise, averaging reduces the standard deviation by the square root of n, where n is the number of averaged observations.

The measuring speed in direct sensor-to-microcontroller interface depends on the type of calibration used, since the number of charging/discharging phases is different. In single point calibration, if the calibration resistor R_c is in the middle of the measurement range as suggested by [5], the time needed to perform one measurement is:

$$T_{1pc} = 2T_{ch} + 2T_{disch} = 2k_1 CR_p + k(2R_{x\min} + 3\Delta R_x / 2), \tag{12}$$

where k is the sensitivity coefficient defined in (1), k_1 is a charging constant which is usually between 5 to 7, and ΔR_x is the measurement range. A good methodology for determination of the optimal discharge-time constant (sensitivity coefficient k) that results in the best speed/resolution trade-off is described in [8]. Similarly, the time needed to perform one measurement for two point calibration, when $R_{c1}=0.15\Delta R_x$ and $R_{c2}=0.85\Delta R_x$ as suggested by [9] is:

$$T_{2pc} = 3k_1 CR_p + k(3R_{x\min} + 2\Delta R_x), \tag{13}$$

www.czasopisma.pan.pl   PAN   www.journals.pan.pl

Metrol. Meas. Syst., Vol. XX (2013), No. 4, pp. 529–542.

and for the three signals method, when $R_{c1}=0.85\Delta R_x$ it is:

$$T_{3sm} = 3k_1 CR_p + k(2R_{x\min} + 2\Delta R_x + 3R).$$ (14)

Comparing (12), (13) and (14) it is clear that the single point calibration provides the highest measuring speed. This is mainly due to the lower number of measuring phases, two instead of three in two point calibration and three signals method. However, the measuring speed in all calibration techniques is limited by the value of the protection resistor R_p given with:

$$R_p \geq \frac{V_{oh}}{I_{g\max}},$$ (15)

where I_{gmax} is the maximal current sourced by the microcontroller ports. Moreover, in [10] the authors suggest that a higher value of R_p would reduce the noise interference effects affecting the voltage comparison of the input Schmitt trigger port. On the other hand, such high value of R_p could rigorously decrease the measurement speed especially for low resistance sensors i.e. when the duration of the charging and the discharging phases are comparable. To overcome this limitation we propose the circuits given in Fig. 4. The electrical circuit in Fig.4a is a complement to the improved single point calibration given in Fig. 3 and the circuit in Fig. 4b is its implementation in two-point calibration.

In the solutions in Fig. 4, the charging of the capacitor is performed through an external p-type MOSFET transistor T_3. This time, the charging transistor is controlled by one additional output port of the microcontroller P_{o3} in Fig. 4a and P_{o4} in Fig. 4b, while the port P_i is configured as input all the time during the measurements. The equations (12) and (13) are directly applicable to the realizations in Fig. 4 when R_p is substituted by R_{dson} of T_3. Therefore, the value of R_p does not contribute to the duration of the charging phase and in fact this resistor is no longer needed. The improvement of measuring speed will be greater as much as the drain-to-source ON resistance of T_3 gets lower and the following conditions are met:

$$I_p \geq \frac{V_{dd}}{R_{dson}},$$ (16)

$$|V_{lo} - V_{dd}| \geq |V_{TH}|,$$ (17)

where I_p is the peak source current of T_3 and V_{dd} is the power supply voltage. In cases where condition (16) does not hold, an additional shunt resistor to T_3 must be employed. The condition (17) is not very restrictive and is usually fulfilled by most commercial MOSFET's. However, unlike previously, (17) implies that in the implementations in Fig. 4, the charging transistor T_3 is turned-on by a logic "low" signal. Another important parameter that must be considered is the leakage current of T_3. Namely, as discussed in the previous section, a lower leakage current would reduce the nonlinearity of the transfer characteristic. One significant drawback of the solutions in Fig. 4 is the increased number of microcontroller pins.

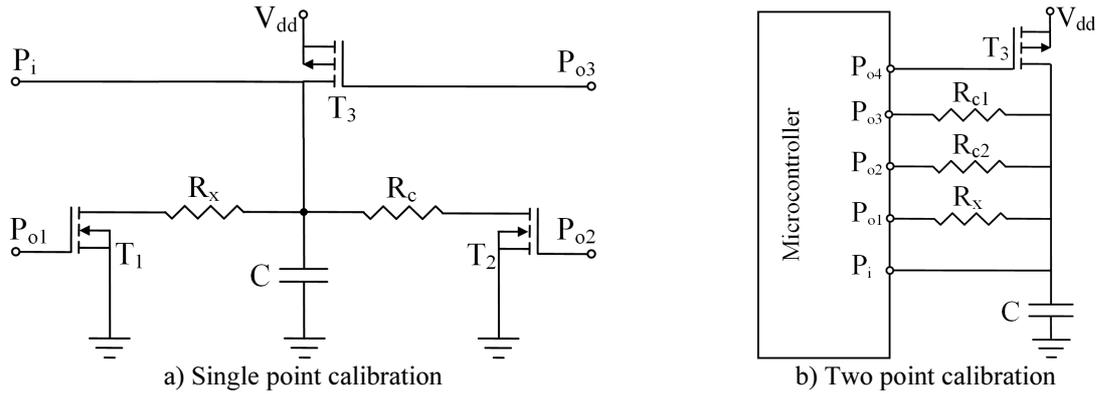a) Single point calibration   b) Two point calibration

Fig. 4. Improving the measuring speed of: a) single point calibration, b) two point calibration.

3.3. Resolution

The performance evaluation of direct sensor-to-microcontroller interface in terms of resolution is performed by analysis of measurement uncertainty. To determine the uncertainty of the measured time period t_x in (3) we use the model as in [7]:

$$Y = X + Z,$$
(18)

where the discharging time t_x is the measurand Y; the resulting value of the time to digital converter multiplied by the time base of the timer T_0 is the observed input quantity X; and Z is correction quantity to take into account the quantization effects. If X and Z are independent, the standard uncertainty of Y will be:

$$u(y) = \sqrt{u^2(x) + u^2(z)}.$$
(19)

The measurement of t_x is affected by noise at the trigger points. Because of this, the input quantity X is random. For Gaussian noise, the root-mean-square (RMS) trigger uncertainty for time interval measurement is [8]:

$$u_{trig} = u(x) = \sqrt{\frac{x^2 + e^2_{nA}}{\left(\dfrac{\Delta V}{\Delta t}\right)^2_A} + \frac{x^2 + e^2_{nB}}{\left(\dfrac{\Delta V}{\Delta t}\right)^2_B}},$$
(20)

where x is the rms noise superimposed on the threshold voltage; e is the noise superimposed on the input signal to be measured; and $\Delta V/\Delta t$ is the slew rate of the signal at the starting (A) or stopping point (B). Since the starting point in direct sensor-to-microcontroller interface is determined by a software trigger, the first A-component in (20) is cancelled. However, the noise components in (20) usually are not specified in the microcontroller datasheets, so the equation (20) cannot be used to quantitatively analyze the uncertainty of X. Therefore, $u(x)$ can be quantitatively analyzed by using type A evaluation i.e. by statistical analysis of a series of observations. Thus, the standard uncertainty of X will be:

$$u(x) = s(X),$$
(21)

www.czasopisma.pan.pl   PAN   www.journals.pan.pl

POLSKA AKADEMIA NAUK

Metrol. Meas. Syst., Vol. XX (2013), No. 4, pp. 529–542.

where $s(X)$ is the standard deviation of a series of independent observations.

The quantization error cannot be evaluated in a measurement because the true value of the measured period is unknown. Generally, the limit error of measurement is between $-T_0$ and T_0, where T_0 is the time base of the timer. All values in this range are equally likely to occur and therefore the quantization effects are modeled by uniform distribution. When the start of the measured time interval is synchronous with the clock, as in the case with direct sensor-to-microcontroller interface, only the end of the period is affected by quantization. The corresponding quantization uncertainty is [11]:

$$u(z) = \frac{T_0}{\sqrt{12}}. \tag{22}$$

Finally, to calculate the effective number of resolution bits (ENOB) we use the equation proposed in [8]:

$$ENOB = N - \log_2\left(\frac{u_{\max}(y)}{u(z)}\right), \tag{23}$$

where $u_{max}(y)$ is the standard uncertainty (19) for the maximal sensor resistance R_{xmax} and N is the resolution (in bits) of the time to digital conversion when only quantization effects are considered, given with:

$$N = \log_2\left(\frac{t_{x\max} - t_{x\min}}{T_0}\right). \tag{24}$$

From (23) it can be seen that ENOB depends on the uncertainties defined with (20) and (22). Since for a given time base (22) is constant, the improvements in resolution can be achieved by reducing (20). Having this in mind, to improve the ENOB of the measurements we propose the circuits shown in Fig. 5. The circuit in Fig. 5a incorporates all improvements of the single point calibration technique elaborated in the previous sections, while Fig. 5b illustrates an improved implementation of the two point calibration.

The modifications proposed in both circuits in Fig. 5 are mainly related to the input module i.e. to the way the capacitor voltage is interfaced to the microcontroller. Normally the capacitor voltage comparison is performed by a Schmitt trigger port of the microcontroller. In such cases, the authors in [1] showed that the microcontroller generates additional noise during the program execution and increases the noise components in (20). As suggested in [1], these effects can be reduced by putting the microcontroller into sleep mode, which is not always practical. Apart from that, the realizations in Fig. 5 incorporate an additional comparator in between the capacitor and the input digital port. Hence, the voltage comparison is not affected by program-related noise but only by the noise of the reference voltage and power supply, which can be controlled by careful electronic design. An additional improvement in the circuit in Fig. 5a is the possibility to charge the capacitor to a higher voltage V and by that to increase N and consequently ENOB in (23). Moreover, the signal conditioning circuit in Fig. 5a is completely isolated from the microcontroller ports i.e. the parameters of T_1, T_2, T_3 and K determine the metrological performances and not those of the microcontroller ports.

Similar solutions to increase the resolution of the measurements by adding an external Schmitt trigger are analyzed in [1].
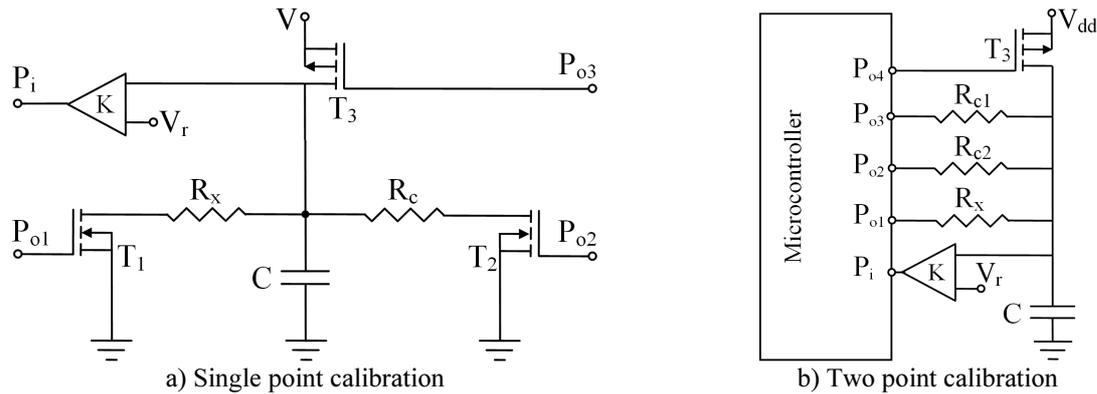
a) Single point calibration   b) Two point calibration
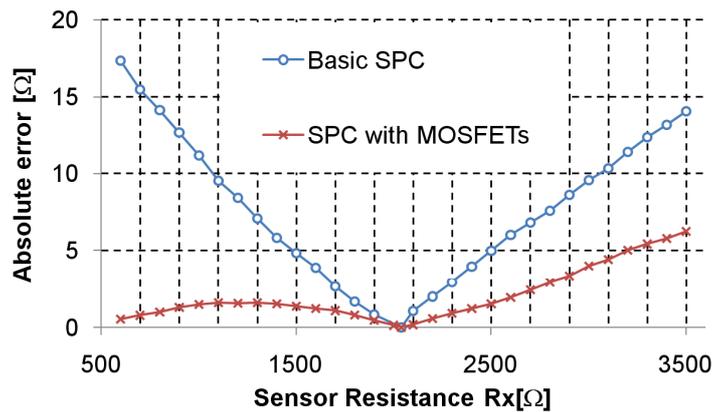
Fig. 5. Improving the resolution of the measurements.

4. Experimental results and discussion

The experiments were realized by using the PIC16F877 microcontroller [12] from Microchip supplied with a 9V battery supply through a L78L05AC voltage regulator. As recommended by the manufacturer, a decoupling capacitor of 100nF was placed as close as possible to the microcontroller power supply pins. The microcontroller clock was from an 8 MHz crystal oscillator resulting in an effective time base of 0.5 μs. The functions of microcontroller ports P_{o1} to P_{o4} and P_i were implemented by RB1 to RB4 and RB0 respectively. The discharging interval was measured with the embedded 16-bit Timer 1, which is stopped when P_i registers an interrupt on the falling edge through the Schmitt trigger buffer of RB0. The measurement data were transferred to a personal computer by using the serial RS232 port and a MAX232 logic level translator which was supplied from a separate power supply to eliminate possible noise interference.
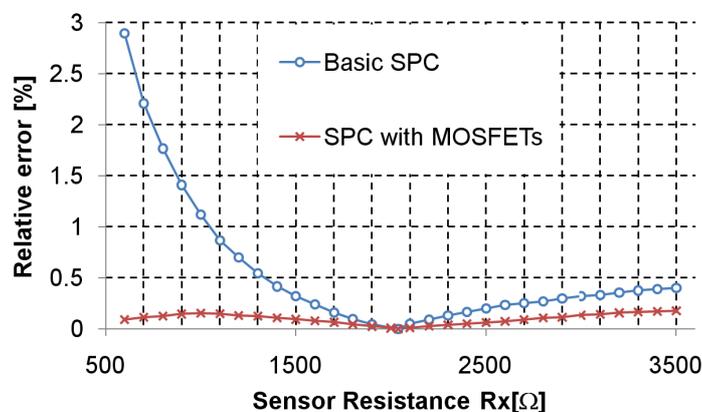
To analyze the accuracy of the single point calibration technique applied to the basic direct sensor-to-microcontroller interface given in Fig. 2a, the transfer characteristic was measured in the range typical for PT1000 resistive temperature sensors from R_{xmin}=600 Ω to R_{xmax}=3500 Ω, as in [5]. The calibration resistor was 2037.8 Ω ±0.2 Ω, which is near the middle of the measurement range [5]. The value of the protection resistor R_p was 996.2 Ω and the nominal value of the capacitor C was 4.7 μF. The sensor resistance was obtained from a Fluke 5500A calibrator with an absolute uncertainty of ±0.06 Ω.

When measuring the transfer characteristic of the single point calibration with the basic circuit given in Fig. 2a, we obtained nearly twice lower systematic errors compared to those reported in [5]. This is because in [5] the authors use the charging interval to measure the sensor resistance instead of the discharging interval used here. In such situation, the output resistance of the microcontroller port driving a logic "high" is much higher (R_{oh}=74.3 Ω) than when driving a logic "low" (R_{ol}=27.01 Ω). The absolute errors of the measurements are given in Fig. 6a and the relative in Fig. 6b. As expected, the absolute errors were minimal near the calibration resistor value and they were symmetrical at the beginning and at the end of the measurement range. The maximal absolute error was 17 Ω resulting in a relative error of 2.8% at the beginning of the measurement range.

When we implemented the single point calibration to the improved circuit given in Fig. 3, the absolute errors were reduced more than twice and the relative errors reduced more than fifteen times compared to the basic circuit in Fig. 2a. The maximal absolute error at the end of the measurement range was around 6 Ω, and the maximal relative errors were 0.18% at the beginning and at the end of the measurement range which is a remarkable error reduction with only a minor hardware improvement.

www.czasopisma.pan.pl   PAN   www.journals.pan.pl

Metrol. Meas. Syst., Vol. XX (2013), No. 4, pp. 529–542.

a)   Absolute errors

b)   Relative errors

Fig. 6. Systematic errors of the single point calibration.

For realization of the circuit given in Fig. 3, T_1 and T_2 were implemented by using an IRF7311 [13] dual N-MOS transistor with a low drain-to-source ON resistance of 30 mΩ and low leakage current of 1 µA at the ambient temperature of 25 °C. Such a low value for R_{dson} provides condition (10) to be quite reasonable. Hence, (7) becomes $R_{x1p}=0.987R_x + 26.6$, and (9) becomes $R_{x1p}=0.99998R_x + 0.0299$ which once again confirms the great reduction of the gain and offset components. The leakage currents of the MOSFET transistors in IRF7311 are on the same order compared to those of the PIC16F877 ports and therefore the nonlinearity effects in both circuits in Fig. 2a and Fig. 3 are similar. Having in mind that the maximum current sunk by the microcontroller ports of PIC16F877 is 25mA, according to (11), the minimal sensor resistance that can be measured with the circuit given in Fig. 2a is 200 Ω. On the other hand, the maximal continuous drain current of IRF7311 in [13] is 5.3 A, which according to (11) allows measurement of sensor resistances down to 1 Ω as long as such high pulse current does not damage the sensor or exceed the maximal allowed dissipation (self-heating).

To evaluate the speed performance of each calibration technique we have analyzed the same measurement range as in the previous example. The measured values of the external components used for implementation of the circuits given in Fig. 2a, Fig. 2b and Fig. 2c are given in Table 1, and the measured microcontroller parameters are summarized in Table. 2.

The values of R and R_p in Table 1 were chosen as low as possible to ensure highest speed and to fulfil the condition (15).

Table 1. Measured values of the external electrical components.

Parameter	R_c [Ω]	R_{c1} [Ω]	R_{c2} [Ω]	R_p [Ω]	R [Ω]	C [μF]
Measured value	2037.8	1028.7	3029.2	216.1	223.7	4.73

Table 2. Measured parameters of the microcontroller PIC16F877.

Parameter	V_{dd} [V]	V_{ol} [mV]	V_{oh} [V]	V_{tl} [V]	R_{ol} [Ω]
Measured value	5.10	5.2	5.10	1.458	27.01

To realize the improved circuits given in Fig. 4a and Fig. 4b, for the transistor T_3 we have used a p-channel MOS transistor BS250 [14] with a drain-to-source ON resistance around 10 Ω and a continuous drain current of 250 mA. Hence, according (16), an additional shunt resistor with a nominal value of 10 Ω had to be used in series with T_3. The maximal gate threshold voltage of the transistor BS250 in [14] is V_{TH}=3.5 V which fulfils the condition (17). Having in mind the measured microcontroller parameters in Table 2, the sensitivity coefficient in (12), (13) and (14) is k =5.93·10^{-6}. Hence, by selecting k_1=7 and by using the values given in Table 1, the time intervals needed to perform one measurement for each calibration technique given with (12), (13) and (14) for all realizations in Fig. 2 and Fig. 4 are given in Table 3.
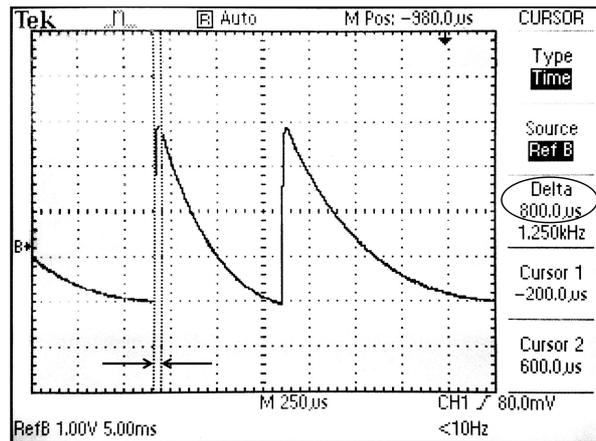
Table 3. Time needed to perform one measurement for each calibration technique.

Parameter	Single point calibration T_{1pc} [ms]	Two point calibration T_{2pc} [ms]	Three signals method T_{3pc} [ms]
Basic circuits (Fig.2)	47.22	66.52	66.94
Improved circuits (Fig.4)	34.23	47.06	47.46

The results reported in Table 3 show that using an external charging transistor increases the measuring speed around 27% for single point calibration and around 29% for the two point calibration and the three signals method in the measuring range of the PT1000 temperature sensor. The improvements in speed will be even better for sensors with lower resistance. The increased speed is mainly due to the reduced charging period T_{ch} in (12) which in this case decreases from 7.15 ms (Fig. 7a) to 0.7 ms (Fig. 7b) when using a charging transistor.

a)   Basic single point calibration

www.czasopisma.pan.pl　　PAN　　www.journals.pan.pl
POLSKA AKADEMIA NAUK

Metrol. Meas. Syst., Vol. XX (2013), No. 4, pp. 529–542.

b) SPC with charging transistor and comparator

Fig. 7. Capacitor voltage in the charging and discharging phase for single point calibration.

To analyze the improvements in resolution, the circuit given in Fig. 5a was tested in two scenarios: with and without an external comparator. The analyses were performed for the measurement range of the PT1000 sensor with a large discharging time constant (C=10 μF) to emphasise the trigger uncertainty given by (20). When the measurements were performed without the external comparator, the standard deviation of 100 readings for the maximal sensor resistance was 6.25 μs which is the trigger uncertainty given by (21). The histogram of the measurements showed that 73% of the observations were one standard deviation ($\pm 1\sigma$) from the mean, 96.5% were between $\pm 2\sigma$ and 99.8% between $\pm 3\sigma$. This suggests that the shape of the histogram is roughly Gaussian and that the trigger voltage comparison is really affected by noise, as expected from (20). Having in mind that the quantization uncertainty for a 2 MHz time base given with (22) is 0.144 μs, the ENOB according (23) is 10.5 bits. In the second example, the capacitor voltage was interfaced to the microcontroller through the MAX 921 comparator [15] supplied from the same power supply of the microcontroller. This comparator has an internal voltage reference of 1.18 V which is lower than the microcontroller threshold voltage given in Table 2. Therefore, the discharging period is longer for the same time constant (Fig. 7b) which increases the resolution N given with (25). In this example, the standard deviation of 100 observations was 3.3 μs which increases the ENOB to 11.7 bits. This confirms that the trigger uncertainty is affected by program execution which is suppressed when an external comparator is used. However, the external comparator will not bring such improvements when using microcontrollers which are able to enter into a sleep mode while waiting for the interrupt, as in [8]. When the comparator was supplied from an external power supply different than that for the microcontroller, the standard deviation reduced to 3.0 μs offering an ENOB of 11.84 bits.

5. Conclusions

Hardware solutions for improving the performance of direct sensor-to-microcontroller interface circuits were presented. The improvements are in increasing the accuracy, speed and resolution of the measurements for different calibration techniques. The analyses were performed in the measurement range of PT1000 resistive temperature sensors. It has been shown that the relative error of the transfer characteristic in single point calibration reduces from 2.8% to 0.18% by employing two external MOSFET transistors. Moreover, such solution allows direct measurement of a sensor having a very low resistance. The speed of the measurement can be increased approximately by 30% for all calibration techniques at

the cost of one additional charging transistor driven by one additional microcontroller pin. The improvements of the measurement speed will be even better for sensors with lower resistance. The experiments confirmed that using an external comparator increases the ENOB of the measurements. In the realization proposed in this paper the ENOB of the measurements increased by 1.3 bits.

References

[1] Reverter, F., Areny, R. P. (2005), *Direct sensor to microcontroller interface circuits*, Barcelona: Marcombo S.A.

[2] Bengtsson, L. E. (2012), Analysis of direct sensor-to-embedded systems interfacing, *International Journal of Intelligent Mechatronics and Robotics*, (2), 41−56.

[3] Pelegri-Sebastia, J., Garcia-Breijo, E., Ibanez, J., Sogorb, T., Laguarda-Miro, N., Garrigues, J. (2012), Low-cost capacitive humidity sensor for application within flexible RFID labels based on microcontroller systems, *IEEE Trans. Instrum. Meas.*, (61), 545–553.

[4] Sifuentes, E., Casas, O., Pallàs-Areny, R. (2011), Wireless magnetic sensor node for vehicle detection with optical wake-up", *IEEE Sens. J.*, (11), 1669−1676.

[5] Costodio, A., Areny, R. P., Bragos, R. (2001) Error analysis and reduction for a simple sensor-microcontroller interface", *IEEE Trans. Instrum. Meas.*, (50), 1644−1647.

[6] Van der Goes, F. M. L. (1996), Low-Cost Smart Sensor Interfacing", *Delft Univ. of Technol.*, Ph. D dissertation.

[7] Lira, H., Wogel, W. (1997), The evaluation of standard uncertainty in presence of limited resolution of indicating devices, *Meas. Sci. Technol.*, (8), 441−443.

[8] Reverter, F., Areny, R. P. (2004), Effective number of resolution bits in direct sensor-to-microcontroller interfaces", *Meas. Sci. Technol.*, (15), 2157−2162.

[9] Areny, R. P., Jordana, J., Casas, O. (2004), Optimal two-point static calibration of measurement systems with quadratic response", *Rev. Sci. Instrum.*, 75(12), 5016−5111.

[10] Reverter, F., Gasulla, M., Pallas-Areny, R. (2007), Analysis of power supply interference effects on direct sensor-to-microcontroller interfaces", *IEEE Trans. Instrum. Meas.*, (56), 171−177.

[11] Zaworski, L., Chaberski, D., Kowalski, M., Zielinski, M. (2012), Quantization Error in Time-to-Digital Converters", *Metrol. Meas. Syst.*, 12(1), 115−122.

[12] PIC16F87X CMOS Flash Microcontroller, Datasheet for Microchip. *ww1.microchip.com/downloads/en/devicedoc/30292c.pdf.* (2001)

[13] IRF7311 Power MOSFET, Datasheet for International Rectifier, *www.irf.com/product-info/datasheets/data/irf7311.pdf.* (2001 November).

[14] BS250 P-Channel Enhancement Mode Vertical D-MOS Transistor, Datasheet for Philips Semiconductors, (1995 April).

[15] MAX921 Ultra Low-Power Single/Dual-Supply Comparator, Datasheet for Maxim, *http://www.maximintegrated.com/datasheet/index.mvp/id/1218.* (2009 April).